Long-range magnetic ordering of FePc molecules driven by interfacial coupling with antiferromagnetic Cr_2O_3

Michele Capra,[1,*] Marco Marino,[2] Andrea Picone,[1] Alessandro Ferretti,[1] Alessio Giampietri,[1] Franco Ciccacci,[1] Sara Fiori,[3,†] Deepak Dagur,[3,4,‡] Federico Motti,[3] Giovanni Vinai,[3] Giancarlo Panaccione,[3] Elena Molteni,[2] Simona Achilli,[2] Guido Fratesi,[2] and Alberto Brambilla[1,§]

[1]*Dipartimento di Fisica, Politecnico di Milano, Piazza Leonardo da Vinci 32, 20133 Milano, Italy*

[2]*Dipartimento di Fisica "Aldo Pontremoli", Università degli Studi di Milano, Via Giovanni Celoria 16, 20133 Milano, Italy*

[3]*CNR - Istituto Officina dei Materiali (IOM), S.S. 14 km 163.5, 34149 Trieste, Italy*

[4]*Department of Physics, University of Trieste, Via A. Valerio 2, 34127 Trieste, Italy*

(Received 16 December 2024; accepted 29 September 2025; published 24 October 2025)

Interfaces between molecular layers and ferromagnetic materials, named spinterfaces, have been widely studied on account of the intriguing magnetic phenomena associated with the spin-polarized hybrid interface states, and of possible innovative applications. This work starts exploring the opportunities given by coupling molecular layers and antiferromagnetic materials, focusing on the magnetoelectric antiferromagnetic insulator Cr_2O_3. Antiferromagnets are currently of great interest for the future development of spintronics and magnonics applications, since they are stable against external fields and they show dynamic behaviors at much higher frequencies, compared to ferromagnets. On the other hand, interacting with the magnetic structure of an antiferromagnet is more challenging. A possible approach is that of establishing an *antiferromagnetic spinterface*, in such a way that external stimuli acting on the molecular side can influence the substrate magnetic parameters. Self-assembled monolayers of FePc (iron phthalocyanine) are prepared on thin Cr_2O_3 films, and the morphological, structural, electronic, and magnetic properties of the resulting antiferromagnetic spinterface are experimentally and theoretically investigated. We observe flat-lying molecular layers that develop a long-range magnetic ordering of the magnetic moments associated with Fe ions. Our calculations support the conclusion that such ordering is established through the interaction at the interface between FePc and Cr_2O_3.

DOI: 10.1103/2pq1-8x4z

I. INTRODUCTION

Spintronics, which is based on the exploitation of the electron spin to transport and store information, has been playing a very important role for developing nanoscale devices in the last decades [1]. The various efforts of the scientific community to support such development often opened the way for innovative approaches, minded to take advantage of the peculiarities of specific classes of materials [2]. For instance, antiferromagnetic (AF) materials, which have, for a long time, been exploited mainly as pinning layers in exchange-biased layered structures [3], have more recently come in the focus of investigations aimed to exploit special features, like their insensitivity to applied magnetic fields and the THz-regime frequencies of AF spin waves [4–7]. Among AF materials, transition metal oxides represent a widely studied class, on account of their chemical stability and of the relatively high Neél temperatures (usually well-above room temperature) that characterize them [8,9]. Lately, spin waves have been generated and detected in AF oxides, such as NiO [10–12], Fe_2O_3 [13,14], and Cr_2O_3 [15,16], both electronically, thermally, and optically.

Another spintronics-derived research branch is Organic (or Molecular) spintronics, in which molecular materials are coupled to ferromagnetic (FM) ones. The interest in exploiting organic materials for spintronics have initially been stimulated by the long relaxation time of the electron spin, which is expected in light elements due to the small spin orbit coupling. Early studies mainly focused on spin injection and spin-polarized transport in devices such as organic spin valves [17,18], while further developments strongly highlighted the importance of interface effects, not only in influencing spin-transport properties but also in determining new ways by which the properties of both the molecular and the FM layer can be modified and tailored [19–24], hence the term *spinterface* was introduced [25,26]. The hybridized states that develop at an organic/inorganic interface can directly determine the spin-polarized character of the

*Present address: Technische Universität Dortmund, Fakultät Physik, Otto-Hahn-Str. 4, Dortmund 44227, Germany.

†Present address: Catalan Institute of Nanoscience and Nanotechnology (ICN2), Campus UAB, Bellaterra, Barcelona 08193, Spain.

‡Present address: Alba Synchrotron Light Facility, Cerdanyola del Valles 08290, Spain.

§Contact author: alberto.brambilla@polimi.it

interface, as remarkably observed, for instance, in the case of C_{60} adsorbed onto a nonmagnetic Cu surface [27]. Such observations allow researchers to envision molecule-mediated ways of tailoring key magnetic parameters, like magnetic anisotropy in FM materials [28]. Molecules, on their side, offer the opportunity of indirectly interacting with the spinterface by coupling to external means, such as chemical reactions [29,30], optical stimuli [31], electric gating [23], and doping [32]. The possibility of combining different effects in a single fundamental unit opens the appealing possibility of developing multifunction molecular spintronic devices [33] that, given the interface-based approach of molecular spintronics, can potentially be downscaled to the 2D limit [34].

In this work, we advance the novel approach of realizing *antiferromagnetic spinterfaces*, in which the molecular layers are coupled to AF substrates, with the aim of being able to exploit external stimuli to induce responses in the AF substrate (such as the generation and the manipulation of AF spin waves), through spin-polarized hybrid interface states. Among AF transition metal oxides Cr_2O_3, which has a Néel temperature slight above room temperature (RT) in the bulk ($T_N = 308$ K), is characterized by the presence of a stable uncompensated surface magnetic layer [35,36], and can be successfully grown in ultra-high vacuum (UHV) on different substrates [36–38]. Moreover, its electrical insulating and magnetoelectric characters make it a suitable candidate as an active element in spintronic devices [39,40].

Several families of organic molecules have been employed in spinterfaces, ranging from C-based ones like pentacene [41] and C_{60} [42], to quinolines [43], to metal complexes of porphyrins and phthalocyanines [44–46], which in several cases are paramagnetic and develop a long-range magnetic ordering when coupled to FM surfaces. The latter molecules, also thanks to their flat structure, have shown indeed to be well-suited for allowing the manipulation of hybrid interface states through interaction with external means [47]. In this study, we prepared and investigated, both experimentally and theoretically, iron phthalocyanine (FePc) self-assembled monolayers on $Cr_2O_3(0001)$, forming the AF spinterface $FePc/Cr_2O_3$. The interaction of metal-phthalocyanine (MPc) molecules on oxide surfaces is much less investigated when compared to MPc adsorbed on metallic surfaces, also on account of the weaker interaction, that might hinder long-range molecular ordering of molecules [48]. On the other hand, a number of investigations have shown that oxygen passivation of FM metallic surfaces is beneficial for the stabilization of well-ordered molecular layers, preserving and possibly enhancing the interfacial magnetic coupling [49–53]. Here, we observe that FePc forms a two-dimensional layer, in which the molecules lay flat on the surface. This self-assembled monolayer appear to be formed on account of the interaction with the substrate, as for thicker layers the molecules start to be tilted out-of-plane. The coupling that develops at the interface is such that a long-range FM ordering of the magnetic moments of the molecular Fe core is achieved. Such AF spinterface is therefore a perfect candidate for development and potential application in AF molecular spintronics.

II. METHODS

A. Experimental details

The experiments were performed in two different UHV systems (base pressure $<2 \times 10^{-10}$ mbar) at Politecnico di Milano and at the NFFA APE-HE beamline of the Elettra Synchrotron radiation facility [54]. All the samples were grown and measured *in situ*. Cu(110) substrates were cleaned by subsequent cycles of sputtering with 1.5 keV Ar^+ ions for 40 minutes, with the sample kept at 480 °C, followed by an annealing at 480 °C for 15 minutes. Ultrathin films of Cr_2O_3 with thickness up to 2.5 nm were grown by reactive molecular beam epitaxy (MBE), in a molecular oxygen atmosphere with $p_{O_2} = 1 \times 10^{-6}$ mbar at 435 °C, followed by 1 minute cooling in oxygen atmosphere. The chromium deposition rate, measured by means of a quartz microbalance, was of about 0.3 nm/min. Iron(II) phthalocyanine (FePc) has been evaporated by MBE, using a powder source, on the $Cr_2O_3/Cu(110)$ system kept at RT.

Auger Electron Spectroscopy (AES) spectra and Low Energy Electron Diffraction (LEED) patterns were collected using an Omicron SPECTALEED with a total acceptance angle of 102°. LEED images have been acquired using a Canon EOS 2000D camera, keeping the focus and zoom fixed for all the images. Scanning Tunneling Microscopy (STM) images were acquired with an Omicron Q-PLUS variable temperature microscope at RT in constant current mode. Q-PLUS tips were purchased directly from Scienta Omicron. X-ray Absorption Spectroscopy (XAS) and X-ray Magnetic Circular Dichroism (XMCD) measurements were taken at the APE-HE beamline. XAS measurements at the Cr $L_{2,3}$ and at the Fe $L_{2,3}$ edges were taken in the Total Electron Yield (TEY) mode, which is characterized by a typical depth sensitivity of the order of 10 nm, with either linear or circular polarizations, at both RT and at 100 K. XMCD spectra were obtained as the difference between two spectra taken with opposite helicities, taking into account a circularity degree of 75%.

B. Computational details

The ground state and its properties are studied through the Density Functional Theory approach, as implemented in the Quantum-Espresso distribution [55,56]. Van der Waals xc-functionals (vdW-DF-c09) [57] and Hubbard U corrections (in the Dudarev's formulation) [58] with an effective U of 4.00 eV for the Cr [59] and of 5.00 eV for the Fe atom [60], are adopted. Variations of the U parameters of ± 1 eV do not alter our conclusions regarding the AF coupling between molecules and substrate in the optimized adsorption geometry (see Table I in the Supplemental Material (SM) [61] and the references cited therein [59,60]). Vanderbilt ultrasoft pseudopotentials (GBRV) [62] with semi-core corrections, and cutoffs of 45 Ry and 270 Ry, respectively, on the wave function and the charge-density, are considered. A 4×4 supercell is built from a primitive cell of the (1×1) O-terminated $Cr_2O_3(0001)$. We sample the surface Brillouin zone by the Gamma point. Four Cr-3O-Cr trilayers (with an overall thickness of $\simeq$5 Å) are considered, with the bottom one kept fixed in structural optimizations. This cell allows us to study diluted FePc molecules, where the distance between the Fe centers of

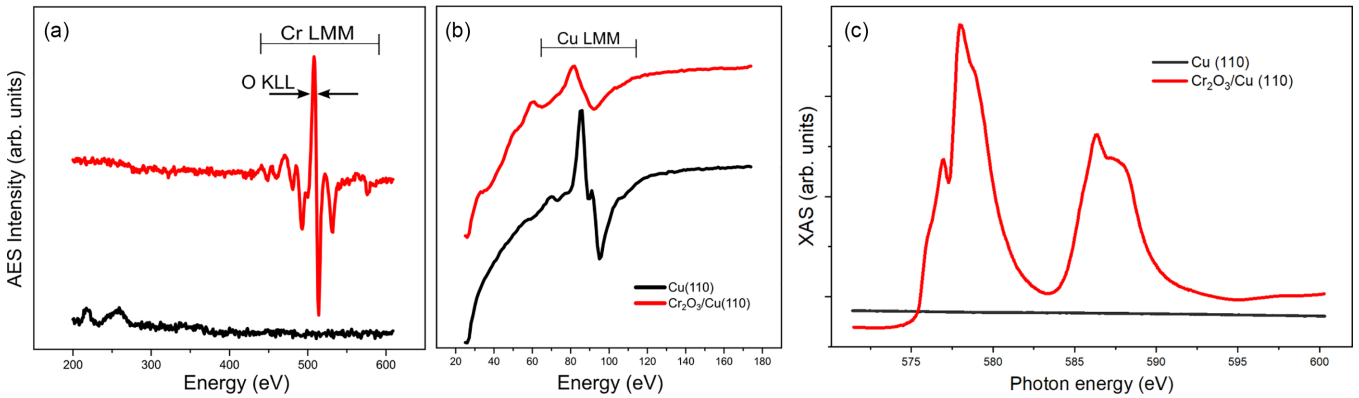

FIG. 1. (a) High energy and (b) low energy AES spectra before and after deposition of 1.2 nm of chromium oxide; (c) XAS spectra before and after deposition of chromium oxide.

two nearby molecules is 20.4 Å, and that between facing H atoms is no smaller than 5.5 Å in the most energetically stable case.

III. RESULTS AND DISCUSSION

A. Experimental results

The stoichiometry of the deposited chromium oxide thin films was validated by means of AES and XAS. In Figs. 1(a) and 1(b), the AES spectra associated with Cr LMM, O KLL, and Cu LMM transitions are shown, in two different energy windows. These spectra testify the successful growth of the desired amount of oxide. Figure 1(c) reports the XAS spectra taken, in linear polarization, at the Cr $L_{2,3}$ edges before and after deposition. Comparing its lineshape with literature [63–65], we confirm that we have stabilized the Cr_2O_3 phase. We underline that all electron spectroscopies measurements realized during the growth processes confirmed the absence of doping and chemical defects in the films.

The structure and morphology of the system has been studied through LEED and STM. In Fig. 2, the LEED patterns of the Cu(110) surface and of Cr_2O_3 on Cu(110) for different coverages are shown. The pristine Cu(110) is characterized by lattice constants $a_{100} = 0.360$ nm and $a_{110} = 0.255$ nm, while the lattice constant of bulk $Cr_2O_3(0001)$ is $a_{ox,b} = 0.496$ nm, measured as the in-plane distance between Cr atoms [38,66]. In Figs. 2(b) and 2(c), the LEED patterns are seen to change upon deposition of, respectively, 1.2 nm and 2.5 nm of Cr_2O_3, displaying hexagonal patterns, rotated by 90 degrees with respect to each other, consistently with the formation of $Cr_2O_3(0001)$ on top of the rectangular Cu(110) surface. In Fig. 2(d), the LEED patterns of the pristine Cu(110) and the 2.5-nm-thick Cr_2O_3 film are compared. We observe that the distance from the center between the first order diffraction spots, in the reciprocal space, is the same for both Cr_2O_3 and Cu(110). We can, therefore, derive the following relationships:

$$b_{ox} \cong b_2 \Longrightarrow \frac{2\pi}{a_{ox,s}\sin\left(\frac{\pi}{3}\right)} \cong \frac{2\pi}{a_{110}}$$

$$\Longrightarrow a_{ox,s} \cong \frac{2}{\sqrt{3}} a_{110} = 0.295 \text{ nm}.$$

This calculated periodicity of the Cr_2O_3 surface $a_{ox,s}$ is, thus, quite different with respect to that of the bulk and, in a previous work on the growth of Cr_2O_3 on Cu(110), it has been associated with the formation of CrO [67]. However, as already mentioned above, the lineshape of the XAS spectrum in Fig. 1(c) can clearly be associated with Cr_2O_3. We have, therefore, to exclude stoichiometry as the origin of such discrepancy, which is instead to be understood in terms of a surface reconstruction.

In fact, by allowing for a mild tensile strain of about 2.8% for $a_{ox,b}$, the Cr_2O_3 crystal can grow commensurately along the [110] direction of the substrate, with a lattice constant about twice a_{110}, keeping the (0001) surface exposed. The periodicity estimated from the LEED pattern discussed above

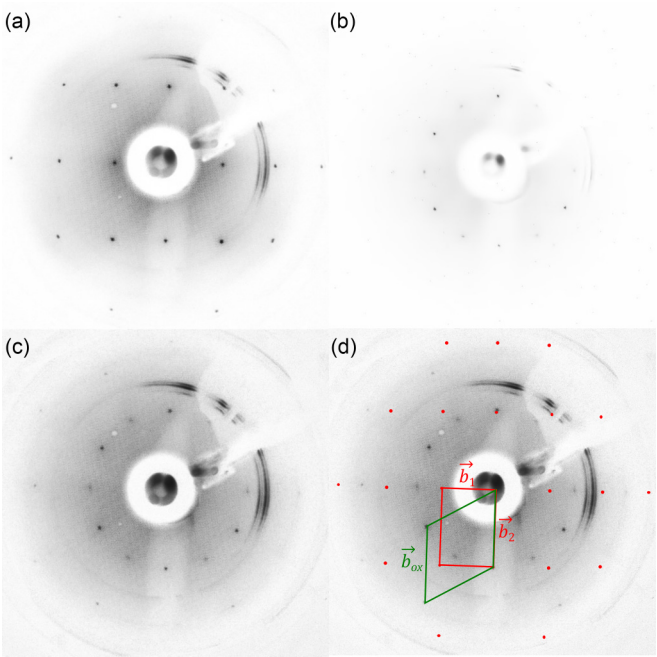

FIG. 2. LEED patterns taken at $E = 175$ eV on: (a) clean Cu(110); (b) 1.2 nm-thick Cr_2O_3 on Cu(110); (c) 2.5 nm-thick Cr_2O_3 on Cu(110). (d) Comparison between (a) and (c) LEED patterns, with corresponding reciprocal unit cells, in red for Cu(110) and in green for Cr_2O_3/Cu(110).

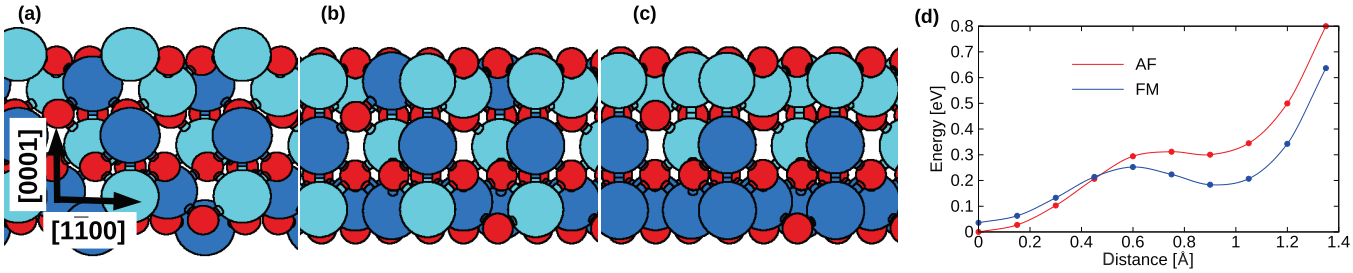

FIG. 3. Side-view of the: (a) Cr-terminated surface; (b) Cr-rich O-terminated surface with AF ordering; (c) Cr-rich O-terminated surface with FM ordering. Color scheme as follows: light and dark blue represent spin-up and spin-down Cr atoms; red represents O. (d) Energy spent in pushing inwards (Δz) the Cr atoms of the Cr-terminated surface seen in panel (a), differentiating between the two possible magnetic orderings of the outer layers, obtaining the two local minima depicted in panels (b) and (c) (per formula unit).

suggests to conclude that the oxide surface is reconstructed by forming the so-called Cr-rich O-terminated surface [38,66]. The "Cr-rich" specification follows the need to distinguish this structure from the nonstoichiometric O-termination that would result by removing the topmost Cr atoms in the Cr-terminated case.

The stability of the surface termination proposed by our experimental diffraction studies is also supported by our DFT calculations. In Fig. 3, we propose indeed a model based on the calculated strained unit cell for chromium oxide. Two different $Cr_2O_3(0001)$ surfaces have been simulated: a Cr-terminated one that results from cutting the crystal between two Cr_2O_3 trilayers (i.e., alternating Cr-O-Cr planes), and the Cr-rich O-terminated one mentioned above.

To simulate the latter configuration, we have started from the Cr-terminated surface, and pushed the top Cr atoms (Cr1) inward (Δz), performing a structural optimization in which the vertical coordinate of the Cr1 was fixed, and considered two magnetic couplings between the Cr atoms: either AF as in Fig. 3(b) or FM as in Fig. 3(c). We have taken a lateral strain of 2.8%, consistent with the experiments, but qualitatively similar results are obtained by moderate strain variations (e.g., 0−4%).

Therefore, the experimental observation of the Cr-rich O-terminated surface, in combination with our DFT calculations, suggests it as a plausible metastable termination of Cr_2O_3 realized in the sample growth conditions, that we consider in the following as the substrate for the study of FePc adsorption. Theoretical studies of FePc on the Cr-terminated $Cr_2O_3(0001)$ are described in a previous work by some of us [68]. We remark differences in the surface chemistry of the two terminations that are relevant for adsorption properties: the O-terminated surface does not expose protruding Cr atoms, which effectively binds FePc by imide N atoms in the Cr-terminated case [68], and has the different magnetic structure, as depicted in Fig. 3.

In Fig. 4, the STM images of Cr_2O_3 on Cu(110) for different coverages are reported. The growth proceeds by islands. From the early stages, as seen in Fig. 4(a), it is possible to observe the presence of two different island types, with either rounded (A) or elongated (B) shape, the latter developing parallel to the [110] direction.

All islands are flat, with an average height of about 1 nm, as shown in Fig. 4(d), which is consistent with a fully developed Cr_2O_3 unit cell [38,67]. As the coverage increases, as shown in Figs. 4(b) and 4(c), rounded islands increase in size, developing a rectangular shape. Elongated islands tend instead to disappear with increasing coverage. Very likely, a preferential growth along the [110] direction is initially favored, thanks to the good lattice matching along such direction. As soon as the island density increases, rounded ones have more chances to enlarge and become more and more stable, developing well-defined edges preferentially along the [100] direction. These observations are also consistent with the progressive disappearance of one of the two hexagonal domains in the LEED pattern, as seen in Fig. 2.

Figure 5(a) shows an STM image of the low coverage Cr_2O_3/Cu(110) surface after deposition of 1 ML of FePc. One can identify three different types of regions, as follows.

(1) Region 1, supposedly belonging to the bare substrate, shows a periodicity of 0.55 nm along the [110] direction, as seen in the corrugation profile reported below, which is consistent with the $p(2 \times 1)$O reconstruction of the Cu(110) surface, also known as the missing row reconstruction [69]. The oxygen reconstruction is formed during the reactive growth of Cr_2O_3.

(2) Region 2 is related to an area where FePc is directly grown above Cu(110)-$p(2 \times 1)$O; FePc molecules form a layer characterized by a lattice parameter of 1.7 nm along the [100] direction of the substrate, as seen in Fig. 5(b) and in the corrugation profile reported below.

(3) Region 3 consists of the FePc monolayer adsorbed above chromium oxide islands. The in-plane ordering of the FePc molecules on top of Cr_2O_3 seems less defined than what is obtained for molecules adsorbed on top of the oxygen-covered Cu surface, particularly lacking a well-defined orientation of the molecular axis compared to the crystallographic axes. Despite this, the molecules appear to remain substantially flat-lying, which should be beneficial in terms of the formation of spin-polarized hybridized interface states [70,71].

In order to investigate the formation of a spin-polarized hybrid interface state, XMCD measurements have been performed. The XMCD spectra shown in Figs. 5(c) and 5(d) have been acquired at 100 K on a 2 ML-thick FePc layer deposited on a 2.5 nm-thick layer of Cr_2O_3/Cu(110) in order to ensure a full coverage of the copper surface by the oxide. The chosen measurement temperature is well below the typical values reported for the Néel temperature of Cr_2O_3 thin films (reportedly larger than 240 K)

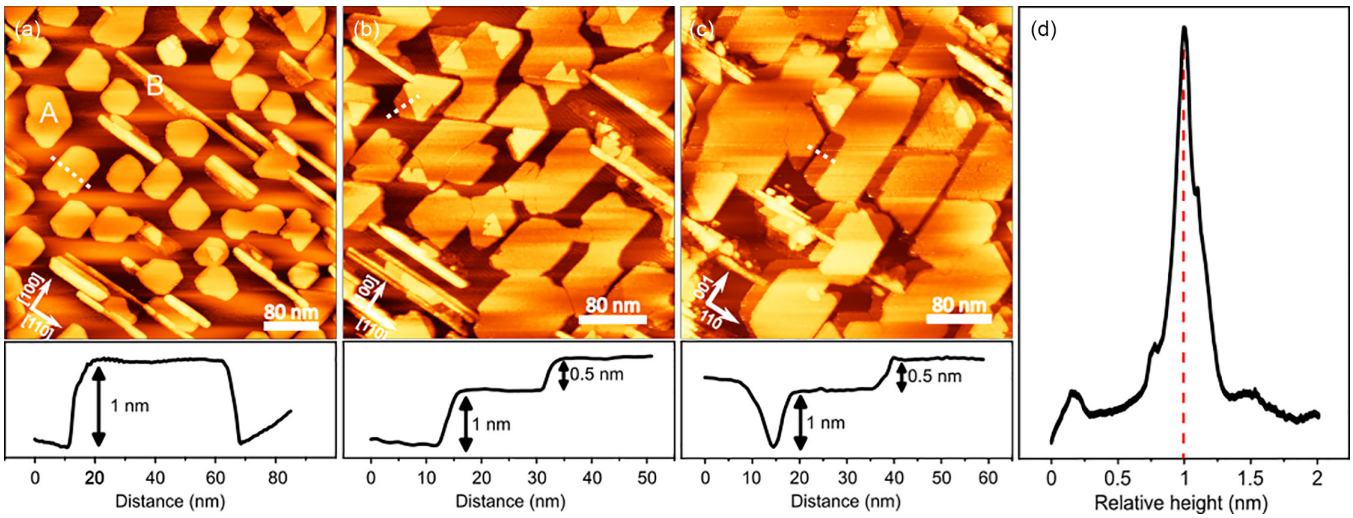

FIG. 4. (a)–(c) STM images of Cr_2O_3 on Cu(110) with thicknesses 0.6 nm, 0.9 nm, and 1.2 nm, respectively. The letters A and B indicate different kind of islands (see text). All images have size $400 \times 400\,\mathrm{nm}^2$ and setpoint $\Delta V = -1.8\,\mathrm{V}$, $I = 0.1\,\mathrm{nA}$. (d) Height histogram of the Cr_2O_3 islands of panel (a).

[36,72–74] The average magnetic moment associated with the Fe ion of the FePc layer has been investigated by measuring the XMCD signal at the Fe $L_{2,3}$ edges, obtained as the difference between two spectra taken with opposite helicities. In Figs. 5(c) and 5(d), absorption spectra for circular left (CL) and circular right (CR) polarizations and the resulting XMCD curve, for x-rays impinging at either $\theta = 45^\circ$ (grazing incidence) or $\theta = 90^\circ$ (normal incidence) are shown.

Analyzing in details the obtained dichroic signal [61], it is possible to extract further information on the direction of the FePc magnetic moment. The main XMCD peaks are associated with the A_1 (705.6 eV) and B_1 (704.8 eV) peaks of the Fe L_3 edge in the absorption spectra, which are related, respectively, to transitions polarized either out-of-plane or in-plane (with respect to the molecular plane), while the signal rising from the A_2 and B_2 peaks is almost negligible or hidden into the noise. At grazing incidence, the resulting XMCD signal has its maximum in correspondence to A_1, with a value of about 1%, and a second peak in correspondence to B_1, with a value of about 0.5%, which is small but still well above the signal-to-noise sensitivity of the beamline (see, e.g., Refs. [75,76]). At normal incidence, only the out-of-plane component is still visible. The presence of two peaks in the dichroic signal, corresponding to two different orientations of the magnetic moment, indicate that the magnetic moment of

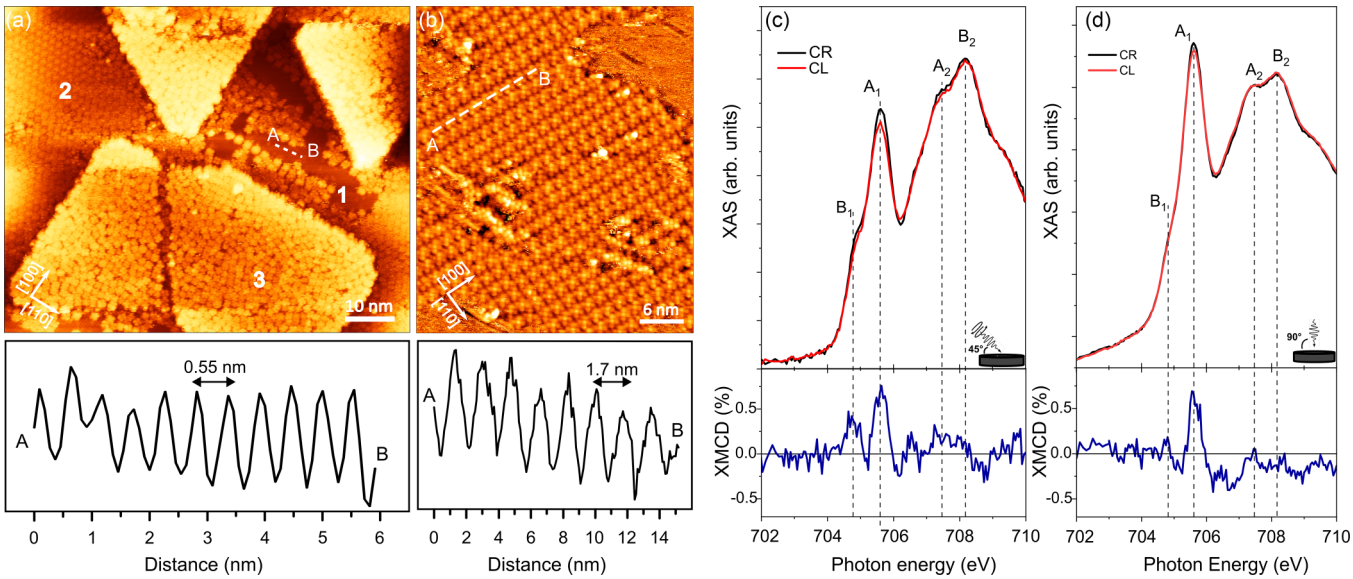

FIG. 5. (a) STM image of 1 ML of FePc on Cr_2O_3/Cu(110); size $90 \times 90\,\mathrm{nm}^2$, setpoint $\Delta V = -2.8\,\mathrm{V}$ $I = 0.1\,\mathrm{nA}$. (b) Zoom on the FePc/Cu(110) region; size $50 \times 50\,\mathrm{nm}^2$, setpoint $\Delta V = -1.5\,\mathrm{V}$, $I = 0.2\,\mathrm{nA}$. The graphs below each STM image report the corrugation profiles taken along the corresponding AB dashed lines. The shown directions refer to the Cu(110) substrate. (c), (d) XAS and XMCD spectra acquired at $T = 100\,\mathrm{K}$ on FePc/Cr_2O_3/Cu(110) at either $\theta = 45^\circ$ (grazing incidence), and $\theta = 90^\circ$ (normal incidence).

TABLE I. Adsorption energy of the considered configurations, in the ferromagnetic (FM) and antiferromagnetic (AF) alignment between Fe and topmost Cr atoms. Values in eV.

Site	Angle	E_{ads}^{FM}	E_{ads}^{AF}	$E_{ads}^{AF} - E_{ads}^{FM}$
Cr1	0°	−3.992	−4.010	−0.018
	45°	−4.085	−4.105	−0.020
Cr2	0°	−3.987	−4.020	−0.033
	45°	−4.114	−4.137	−0.023
Cr3	0°	−4.066	−4.105	−0.039
	45°	−4.185	−4.220	−0.035
O-up	0°	unstable	−4.314	
	15°	−4.419	−4.462	−0.043
	30°	−4.633	−4.677	−0.044
	45°	−4.502	−4.548	−0.047
O-dn	0°	−4.084	−4.107	−0.023
	30°	unstable	−4.101	
	45°	−4.063	−4.079	−0.017

the FePc is not completely lying neither in-plane nor out-of-plane.

The observed XMCD signal therefore testifies the presence of long-range magnetic ordering of spin-polarized states associated with the adsorbed FePc molecules, without a preferential orientation due to the partial molecular disorder. The possible association of the molecular magnetic ordering with that of the substrate is experimentally substantiated by the uniformity of the Cr_2O_3 island heights [see Fig. 4(d)], which would account for a uniform orientation of the magnetization vector in the topmost layer, being the substrate in its AF state at the measurement temperature of 100 K (see also Fig. S2 of the SM [61]. We also underline that, commonly, very high magnetic fields and extremely low temperatures are employed to align the magnetic moments of FePc (and similar paramagnetic molecules) grown onto nonmagnetic substrates [77,78]. In the following section, we will show that our theoretical calculations fully support this interpretation.

As a completion of the XMCD analysis, we have performed the measurements also at the $L_{2,3}$ edges of Cr on the bare Cr_2O_3 substrate, in order to check that, indeed, no detectable XMCD signal could be observed (not shown). This confirms the absence of FM impurities, possibly due to defects or small variations in the stoichiometry, in the AF Cr_2O_3 structure, which could have influenced the magnetic coupling at the interface with the molecules. Furthermore, we verified that the XMCD signal at the Fe edges is observed only in the presence of the molecules, by comparing measurements in the same energy range before and after FePc deposition, as shown in Fig. S3 of the SM [61].

B. Theoretical results

Different adsorption configurations of FePc on the Cr-rich O-terminated $Cr_2O_3(0001)$ are studied. The configurations, reported in Table I, are distinguished by: the angle between the molecular axis and one of the primitive surface axes, the central atom of the adsorption site, and the sign of the magnetic moment of the Fe atom (having set positive "up" spin

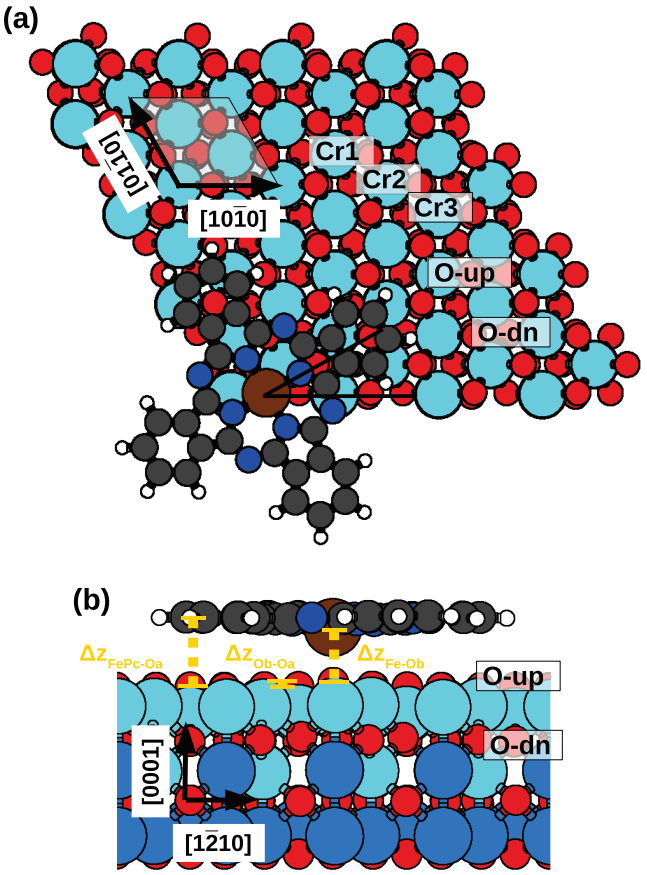

FIG. 6. (a) Top view of the relaxed minimum adsorption energy configuration (O-up 30° FM) of the FePc/Cr_2O_3(0001) spinterface, indicating the angle between the N-Fe-N axis and the surface [10$\bar{1}$0] direction and the unit cell. (b) Its side view, indicating in yellow, respectively, the distance molecule (excluding the Fe atom) O-up layer ($\Delta z_{FePc-Oa}$), the distance Fe O-up atom underneath (Δz_{Fe-Ob}), and the distance of the latter O-up atom and the O-up layer Δz_{Ob-Oa}. Color scheme as in Fig. 3, plus: brown, Fe; dark blue, N; gray, C; white, H. The names of the adsorption sites are directly indicated. In particular, the three Cr and two O atoms, as visible from a top-view of the surface, are differentiated by their respective height, normal to the surface: from top to bottom, O-up, Cr1, Cr2, Cr3, and O-down.

to the surface top layer). In particular, the three Cr and two O atoms visible from a top-view of the surface, as reported in Fig. 6(a), are differentiated by their respective height, normal to the surface. Going inward in the substrate we have O-up, Cr1, Cr2, Cr3, and O-down; of these, the Cr1, Cr2, and Cr3 are polarized in the same direction. In addition, we call the O atom under the Fe atom Ob (b = below) and the O top layer Oa (a = average).

The adsorption energy was calculated, following standard practice, as the difference in total energy between the combined system and the clean substrate and isolated molecule. As reference for the isolated molecule configuration, the Jahn-Teller configuration is considered. The D_{4h} symmetry is broken in favor of a D_{2h} symmetry, with a difference in the nonequivalent Fe-N bond lengths of 0.1%. In particular, in this configuration the magnetic moment of the Fe atom is $2.17\mu_B$, with a d orbital filling $d_{z^2}^{\downarrow} d_{xz}^{\downarrow} d_{yz}^{\uparrow} d_{yz}^{\downarrow} d_{xy}^{\uparrow} d_{xy}^{\downarrow}$ (where we

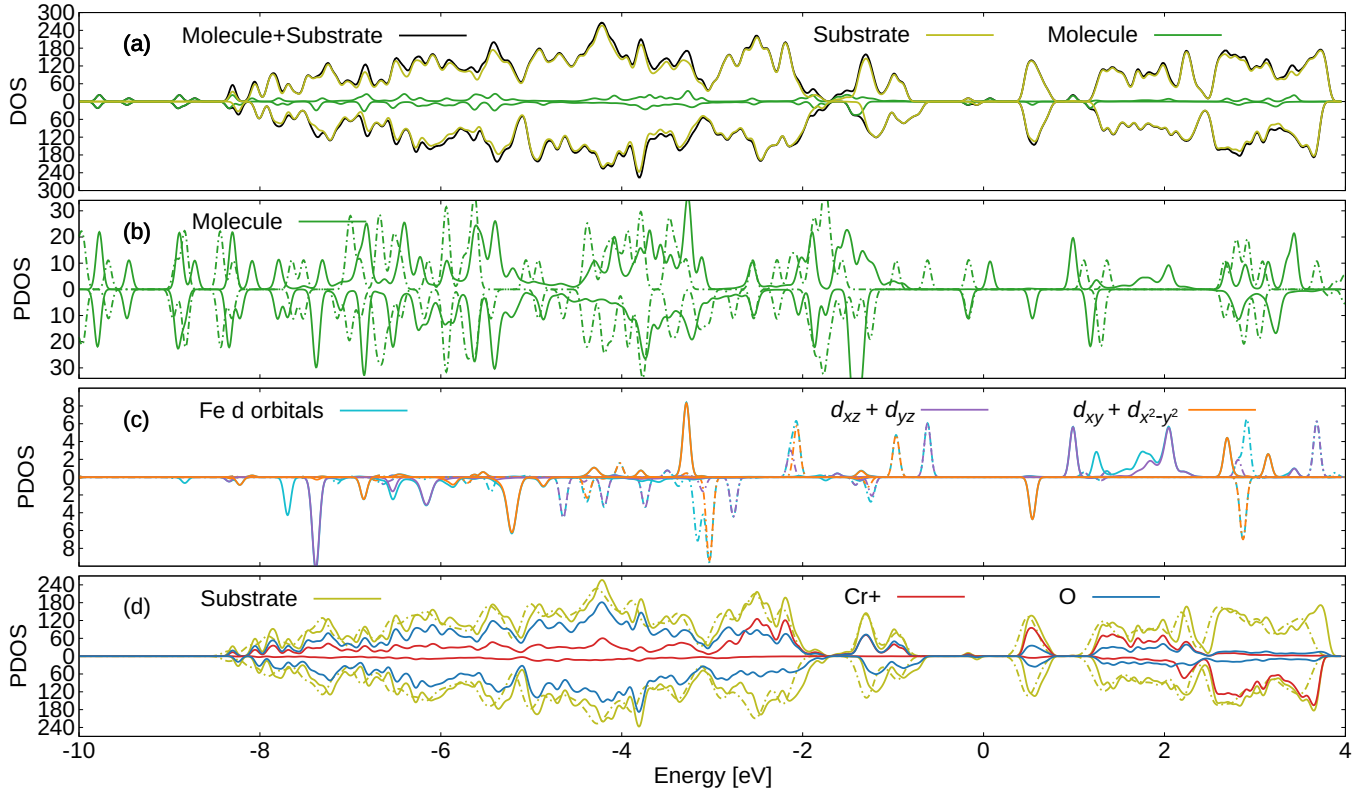

FIG. 7. Electronic DOS (a) and PDOS (b)–(d) of FePc/Cr_2O_3(0001). The PDOS is summed over: (b) all molecule atoms; (c) Fe d orbitals; (d) substrate atoms. Color codes: Light-Green: all substrate atoms; Dark-Green: molecule atoms; Red: Cr atoms of the majority spin channel ("Cr+", *d* orbitals), the minority one being analogous upon switching up/down components; Blue: O atoms; Cyan: Fe atom *d* orbitals; Purple: Fe atom $d_{xz} + d_{yz}$ orbitals; Orange: Fe atom $d_{xy} + d_{x^2-y^2}$ orbitals. Solid/dash-dotted lines indicate adsorbed and gas phase molecules or pristine substrate, respectively. Negative spin components are shown as negative values. All values in states/eV/cell.

take the spin-down component as the majority one to facilitate the comparison with the adsorbed case).

From adsorption energy considerations, a preference for the O-up sites emerges, with a partially rotated configuration, in which one of the in-plane molecular axes forms an angle of 30° with respect to the substrate crystalline direction [10$\bar{1}$0]. For what concerns the magnetic ordering, an AF exchange coupling is established on the different sites and at different angles, probably due to a super-exchange mechanism mediated by the O atoms, with energy differences $E_{\text{ads}}^{\text{AF}} - E_{\text{ads}}^{\text{FM}}$ typically below 50 meV. Such AF coupling of the molecules with respect to the top FM layer (Cr1-Cr2-Cr3) is consistent with the net magnetic signal observed in the XMCD results, having atomically flat terraces of the Cr_2O_3 substrate, with a substantially uniform height (STM Fig. 4).

From a structural point of view, in all the configurations the Fe atom reduces its height with respect to the rest of the molecule [see the side view in Fig. 6(b)]. However, while in the Cr1 and Cr2 configurations the difference is around 0.1 Å and the molecule preserves a flat geometry (the distance of the molecule with the average O-up layer is around $\Delta z_{\text{FePc-Oa}} = 2.8-3.0$ Å), in the other configurations the difference is greater and the atoms around the Fe atom are also lowered: in particular, in the Cr3 configurations the Fe atom reaches an height of $\Delta z_{\text{Fe-Oa}} = 2.6$ Å, with a difference with respect to the the rest of the molecule of 0.3 Å; in the O-dn configurations one has $\Delta z_{\text{Fe-Oa}} = 2.7-2.8$ Å, with a difference of 0.2 Å; in the O-up configurations, $\Delta z_{\text{Fe-Oa}} = 2.4$ Å, with a difference of 0.4 Å (an exception is the O-up at 0° case that is flatter, with $\Delta z_{\text{Fe-Oa}} = 2.7$ Å and a difference of 0.2 Å). The partially dragged atoms are the surrounding pyridinic N atoms (2.7–2.9 Å), which are 0.04 Å lower on average than the imide ones (0.10 Å in the O-up configurations). Additional information on atomic displacements is available in the Fig. S4 of the SM [61].

Thus, the lowering of the adsorption energy can be associated with the lowering of the Fe atom towards the O-up atoms of the surface. In particular, in the most stable O-up configuration at 30°, the Fe atom chemically binds with the top O-up atom below ($\Delta z_{\text{Fe-Ob}} = 2.25$ Å), that in turn is lifted by $\Delta z_{\text{Ob-Oa}} = 0.15$ Å over the average O-up layer of the substrate, see Fig. 6(b). However, the lower Fe atom height is not sufficient to explain the differences in energy between the different angles. In this regards, it appears that lower energies are obtained for those configurations with the in-plane molecular axis along a crystalline direction of the substrate, i.e., in the O-up configuration a rotation of the molecular axis of 30° involves a energy gain of 0.3 eV.

Looking at the the projected density of states (PDOS) of the most stable configuration (O-up 30°) in Fig. 7, a few remarks can be done about the electronic properties of the studied spinterface. In the adsorbed system [see Fig. 7(a)], the presence of a molecular state in the electronic band gap of the pristine substrate has the effect of reducing the gap value: from 1.34 eV

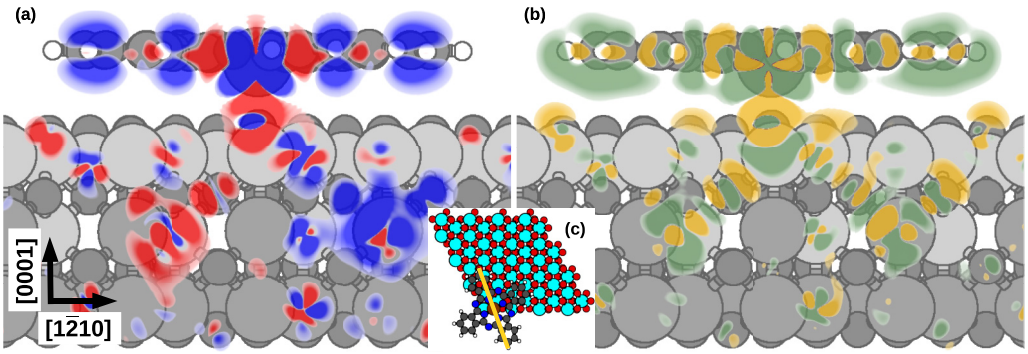

FIG. 8. Side-view of the spin density (a) and charge density variations (b) of the minimum energy adsorption configuration with respect to the isolated systems (full-color regions correspond to values whose modulus exceeds 0.001 bohr^{-3}). The vertical plane on which data is shown is marked in yellow in panel (c) and forms a small angle (10°) with respect to the [01$\bar{1}$0] direction). Red/blue: increase/decrease in spin density; yellow/green: increase/decrease in electron density.

to 0.24 eV in the spin-up channel and from 1.30 to 0.53 eV in the spin-down channel. In the spin-up channel, the highest valence state (located at 0.17 eV below the Fermi energy, as seen in Fig. 7) is of substrate nature, while the lowest conduction state is of molecular nature. In the spin-down channel, instead, the lowest conduction state and the highest valence state (located at 0.07 eV below the Fermi energy) are both of substrate nature.

The broadening and energy shift of the molecular orbitals suggest a significant hybridization with the substrate energy states. However, while the variations of the molecular *sp* orbitals can be related only to a shift of the energy levels, the changes in the Fe *d* orbitals seem to require a more complex interpretation; these, in fact, are due to the spin-crossover of the molecule upon adsorption. Neglecting the Fe atom *d* orbitals hybridization with the N and C atoms *p* orbitals, two electrons populating the $d_{xz} + d_{yz}$ and the d_{xy} orbitals in the spin-up channel (minority) move to the $d_{x^2-y^2} + d_{z^2}$ orbitals in the spin-up and spin-down (majority) channels, with a consequent increase in the absolute value of the Fe magnetic moment, going from $-2.17\mu_B$ to $-3.08\mu_B$. The orbital configuration of the Fe ion changes from $d_{z^2}^{\downarrow}(d_{xz} + d_{yz})^{\downarrow\downarrow\uparrow}(d_{xy} + d_{x^2-y^2})^{\downarrow\uparrow}$ to $d_{z^2}^{\downarrow}(d_{xz} + d_{yz})^{\downarrow\downarrow}(d_{xy} + d_{x^2-y^2})^{1.7\downarrow\,1.5\uparrow}$.

Looking at the spin density variations (on a vertical plane passing through the Fe atom, as shown in Fig. 8(c) with respect to the spin density of the isolated molecule and pristine surface in Fig. 8(b), additional remarks can be done about the magnetic properties of the studied spinterface. A large increase of the (negative) magnetic moment of Fe, and of the magnetic moments of the substrate atoms along the crystalline directions of the substrate, reveals a propagation of the molecule-substrate magnetic interaction to subsurface Cr atoms. Indeed, the magnetic moments of the two sub-surface Cr atoms along the diagonal increases in modulus by $\sim 0.7\mu_B$. These two atoms are linked to the surface ones by super-exchange mechanisms mediated by the O-down atoms. A directionality of the result derives from the alignment of the molecule (i.e., of one of the N-Fe-N axes) with an high-symmetry surface azimuth. More details about magnetic variations can be seen in the Fig. S5 of the SM [61], where we project them onto individual atoms: it appears that the substrate top surface is not significantly affected by the molecule adsorption, apart from small local variations, at variance with the subsurface one.

It is interesting to compare these results with the corresponding charge density variations upon adsorption, reported in Fig. 8(c). The similarity with Fig. 8(b) reveals a direct correlation between changes in magnetic moments and charge. In the substrate, the charge displacement pattern extends to the same subsurface atoms as for the spin density variations. These conclusions are confirmed by a Löwdin analysis, as reported in Fig. S5 of the SM [61]. This analysis, moreover, shows a transfer of 1.5 electrons from the molecule toward the top-layer surface O atoms, with the noticeable exception of the two pyrrolic N along [01$\bar{1}$0], where the electron density increases. In the substrate, the charge displacement pattern extends to the same subsurface atoms as for the spin density variations. The net increase of the magnetic moments therein implies that the charge transfer mainly involves the local majority spin channel (e.g., spin-up, for positively magnetized Cr atoms). Moreover, we note that the asymmetric variations of the magnetic moments of the internal N atoms seem to counterbalance the distortion of the isolated molecule due to the Jahn-Teller effect. In the adsorption, indeed, the molecule is capable of regaining its D_4 symmetry.

Note that, due to the significant number of degrees of freedom, the spinterface can have multiple configurations which differ slightly (of the order of 10^{-2} eV) in the adsorption energy: these are mainly distinguishable in terms of "molecular" orbitals ordering near the Fermi energy. However, the main physical findings of the spinterface are unchanged.

IV. CONCLUSIONS

In summary, we have grown and characterized ultrathin films of the magnetoelectric antiferromagnet Cr_2O_3 on Cu(110), on top of which we prepared the FePc/Cr_2O_3 AF spinterface. In the early stages, the growth of Cr_2O_3 proceeds by islands, which show a rather uniform height and are characterized by a well-ordered atomically flat surface. The resulting Cr_2O_3 surface presents a Cr rich, O-terminated reconstruction, which develops along with a mild tensile strain of 2.8% in the bulk-truncated surface structure of the oxide.

The stability of such reconstruction is also supported by our DFT calculations, which show a local energy minimum for the observed surface structure. A FePc molecular monolayer forms on the reconstructed Cr_2O_3 surface with a substantially flat adsorption geometry, characterized by a poor spatial ordering. The latter observation is also consistent with *ab initio* calculations, which give only small differences in the energy associated with adsorption at different surface sites.

We have also investigated the spin-polarized hybrid states forming at the FePc/Cr_2O_3 AF spinterface by means of XMCD, which testified the occurrence of a long-range ordering of the magnetic moments associated with the Fe ions. Our theoretical calculations support the conclusion that such magnetic ordering is induced by the interaction of the molecules with the magnetically ordered oxide surface. In particular, an antiparallel alignment of the Fe magnetic moments with respect to the top-surface magnetization is found for different adsorption configurations, especially for the most stable ones, as well as an enhancement in their magnitude.

Based on these results, we conclude that the FePc/Cr_2O_3 system represents a paradigmatic example of an AF spinterface. We envision that the spin-polarized hybrid states at such interfaces can be exploited to manipulate the magnetic properties of the underlying AF oxides via external stimuli acting on the molecular side, as already demonstrated for several FM spinterfaces.

ACKNOWLEDGMENTS

This work has received funding from the European Union's Horizon 2020 Research and Innovation Programme under Project SINFONIA, Grant No. 964396. We acknowledge the CINECA award under the ISCRA initiative, for the availability of high performance computing resources and support. This work has been partially performed in the framework of the Nanoscience Foundry and Fine Analysis (NFFA-MUR Italy Progetti Internazionali) project. S.F. and G.V. thank Andrea Fondacaro for technical support during the beamtimes at the APE-HE beamline.

DATA AVAILABILITY

The data that support the findings of this article are openly available [84], embargo periods may apply.

[1] C. Chappert, A. Fert, and F. N. Van Dau, The emergence of spin electronics in data storage, Nat. Mater. **6**, 813 (2007).
[2] A. Hirohata, K. Yamada, Y. Nakatani, I.-L. Prejbeanu, B. Diény, P. Pirro, and B. Hillebrands, Review on spintronics: Principles and device applications, J. Magn. Magn. Mater. **509**, 166711 (2020).
[3] P. Grünberg, Layered magnetic structures: History, highlights, applications, Phys. Today **54**, 31 (2001).
[4] T. Jungwirth, X. Marti, P. Wadley, and J. Wunderlich, Antiferromagnetic spintronics, Nat. Nanotechnol. **11**, 231 (2016).
[5] V. Baltz, A. Manchon, M. Tsoi, T. Moriyama, T. Ono, and Y. Tserkovnyak, Antiferromagnetic spintronics, Rev. Mod. Phys. **90**, 015005 (2018).
[6] H. Meer, O. Gomonay, A. Wittmann, and M. Kläui, Antiferromagnetic insulatronics: Spintronics in insulating 3d metal oxides with antiferromagnetic coupling, Appl. Phys. Lett. **122**, 080502 (2023).
[7] H. Chen, L. Liu, X. Zhou, Z. Meng, X. Wang, Z. Duan, G. Zhao, H. Yan, P. Qin, and Z. Liu, Emerging antiferromagnets for spintronics, Adv. Mater. **36**, 2310379 (2024).
[8] M. Finazzi, L. Duò, and F. Ciccacci, Magnetic properties of interfaces and multilayers based on thin antiferromagnetic oxide films, Surf. Sci. Rep. **64**, 139 (2009).
[9] Edited by L. Duò, M. Finazzi, and F. Ciccacci, *Magnetic Properties of Antiferromagnetic Oxide Materials* (WILEY-VCH Verlag GmbH & Co. KGaA, Weinheim, 2010).
[10] H. Wang, C. Du, P. C. Hammel, and F. Yang, Antiferromagnonic spin transport from $Y_3Fe_5O_{12}$ into NiO, Phys. Rev. Lett. **113**, 097202 (2014).
[11] L. Baldrati, C. Schneider, T. Niizeki, R. Ramos, J. Cramer, A. Ross, E. Saitoh, and M. Kläui, Spin transport in multilayer systems with fully epitaxial NiO thin films, Phys. Rev. B **98**, 014409 (2018).
[12] D. Bossini, M. Pancaldi, L. Soumah, M. Basini, F. Mertens, M. Cinchetti, T. Satoh, O. Gomonay, and S. Bonetti, Ultrafast amplification and nonlinear magnetoelastic coupling of coherent magnon modes in an antiferromagnet, Phys. Rev. Lett. **127**, 077202 (2021).
[13] R. Lebrun, A. Ross, S. A. Bender, A. Qaiumzadeh, L. Baldrati, J. Cramer, A. Brataas, R. A. Duine, and M. Kläui, Tunable long-distance spin transport in a crystalline antiferromagnetic iron oxide, Nature (London) **561**, 222 (2018).
[14] J. Han, P. Zhang, Z. Bi, Y. Fan, T. S. Safi, J. Xiang, J. Finley, L. Fu, R. Cheng, and L. Liu, Birefringence-like spin transport via linearly polarized antiferromagnetic magnons, Nat. Nanotechnol. **15**, 563 (2020).
[15] S. Seki, T. Ideue, M. Kubota, Y. Kozuka, R. Takagi, M. Nakamura, Y. Kaneko, M. Kawasaki, and Y. Tokura, Thermal generation of spin current in an antiferromagnet, Phys. Rev. Lett. **115**, 266601 (2015).
[16] J. Li, C. B. Wilson, R. Cheng, M. Lohmann, M. Kavand, W. Yuan, M. Aldosary, N. Agladze, P. Wei, M. S. Sherwin, and J. Shi, Spin current from sub-terahertz-generated antiferromagnetic magnons, Nature (London) **578**, 70 (2020).
[17] V. A. Dediu, L. E. Hueso, I. Bergenti, and C. Taliani, Spin routes in organic semiconductors, Nat. Mater. **8**, 707 (2009).
[18] D. Sun, E. Ehrenfreund, and Z. V. Vardeny, The first decade of organic spintronics research, Chem. Commun. **50**, 1781 (2014).
[19] C. Barraud, P. Seneor, R. Mattana, S. Fusil, K. Bouzehouane, C. Deranlot, P. Graziosi, L. Hueso, I. Bergenti, V. Dediu, F. Petroff, and A. Fert, Unravelling the role of the interface for spin injection into organic semiconductors, Nat. Phys. **6**, 615 (2010).
[20] S. Sanvito, Molecular spintronics, Chem. Soc. Rev. **40**, 3336 (2011).

[21] D. Ciudad, M. Gobbi, C. J. Kinane, M. Eich, J. S. Moodera, and L. E. Hueso, Sign control of magnetoresistance through chemically engineered interfaces, Adv. Mater. **26**, 7561 (2014).
[22] K. V. Raman, Interface-assisted molecular spintronics, Appl. Phys. Rev. **1**, 031101 (2014).
[23] M. Cinchetti, V. A. Dediu, and L. E. Hueso, Activating the molecular spinterface, Nat. Mater. **16**, 507 (2017).
[24] H.-J. Jang and C. A. Richter, Organic spin-valves and beyond: Spin injection and transport in organic semiconductors and the effect of interfacial engineering, Adv. Mater. **29**, 1602739 (2017).
[25] S. Sanvito, The rise of spinterface science, Nat. Phys. **6**, 562 (2010).
[26] I. Bergenti and V. Dediu, Spinterface: A new platform for spintronics, Nano Mater. Sci. **1**, 149 (2019).
[27] F. A. Ma'Mari, T. Moorsom, G. Teobaldi, W. Deacon, T. Prokscha, H. Luetkens, S. Lee, G. E. Sterbinsky, D. A. Arena, D. A. MacLaren, M. Flokstra, M. Ali, M. C. Wheeler, G. Burnell, B. J. Hickey, and O. Cespedes, Beating the stoner criterion using molecular interfaces, Nature (London) **524**, 69 (2015).
[28] M. Benini, G. Allodi, A. Surpi, A. Riminucci, K.-W. Lin, S. Sanna, V. A. Dediu, and I. Bergenti, In-depth NMR investigation of the magnetic hardening in Co thin films induced by the interface with molecular layers, Adv. Mater. Interfaces **9**, 2201394 (2022).
[29] C. Wäckerlin, D. Chylarecka, A. Kleibert, K. Müller, C. Iacovita, F. Nolting, T. A. Jung, and N. Ballav, Controlling spins in adsorbed molecules by a chemical switch, Nat. Commun. **1**, 61 (2010).
[30] C. Wäckerlin, K. Tarafder, D. Siewert, J. Girovsky, T. Hählen, C. Iacovita, A. Kleibert, F. Nolting, T. A. Jung, P. M. Oppeneer, and N. Ballav, On-surface coordination chemistry of planar molecular spin systems: Novel magnetochemical effects induced by axial ligands, Chem. Sci. **3**, 3154 (2012).
[31] A. Domínguez-Celorrio, C. Garcia-Fernandez, S. Quiroga, P. Koval, V. Langlais, D. Peña, D. Sánchez-Portal, D. Serrate, and J. Lobo-Checa, On-surface synthesis of Mn-phthalocyanines with optically active ligands, Nanoscale **14**, 8069 (2022).
[32] G. Avvisati, P. Gargiani, C. Mariani, and M. G. Betti, Tuning the magnetic coupling of a molecular spin interface via electron doping, Nano Lett. **21**, 666 (2021).
[33] L. Guo, X. Gu, X. Zhu, and X. Sun, Recent advances in molecular spintronics: Multifunctional spintronic devices, Adv. Mater. **31**, 1805355 (2019).
[34] M. Gobbi, E. Orgiu, and P. Samorí, When 2D materials meet molecules: Opportunities and challenges of hybrid organic/inorganic van der Waals heterostructures, Adv. Mater. **30**, 1706103 (2018).
[35] X. He, Y. Wang, N. Wu, A. N. Caruso, E. Vescovo, K. D. Belashchenko, P. A. Dowben, and C. Binek, Robust isothermal electric control of exchange bias at room temperature, Nat. Mater. **9**, 579 (2010).
[36] N. Wu, X. He, A. L. Wysocki, U. Lanke, T. Komesu, K. D. Belashchenko, C. Binek, and P. A. Dowben, Imaging and control of surface magnetization domains in a magnetoelectric antiferromagnet, Phys. Rev. Lett. **106**, 087202 (2011).
[37] S. Cao, X. Zhang, N. Wu, A. T. N'Diaye, G. Chen, A. K. Schmid, X. Chen, W. Echtenkamp, A. Enders, C. Binek, and P. A. Dowben, Spin polarization asymmetry at the surface of chromia, New J. Phys. **16**, 073021 (2014).
[38] A. Lodesani, A. Picone, A. Brambilla, D. Giannotti, M. S. Jagadeesh, A. Calloni, G. Bussetti, G. Berti, M. Zani, M. Finazzi, L. Duò, and F. Ciccacci, Graphene as an ideal buffer layer for the growth of high-quality ultrathin Cr_2O_3 layers on Ni(111), ACS Nano **13**, 4361 (2019).
[39] T. Kosub, M. Kopte, F. Radu, O. G. Schmidt, and D. Makarov, All-electric access to the magnetic-field-invariant magnetization of antiferromagnets, Phys. Rev. Lett. **115**, 097201 (2015).
[40] T. Kosub, M. Kopte, R. Hühne, P. Appel, B. Shields, P. Maletinsky, R. Hübner, M. O. Liedke, J. Fassbender, O. G. Schmidt, and D. Makarov, Purely antiferromagnetic magnetoelectric random access memory, Nat. Commun. **8**, 13985 (2017).
[41] Y.-H. Chu, C.-H. Hsu, C.-I. Lu, H.-H. Yang, T.-H. Yang, C.-H. Luo, K.-J. Yang, S.-H. Hsu, G. Hoffmann, C.-C. Kaun, and M.-T. Lin, Spin-Dependent molecule symmetry at a pentacene–co spinterface, ACS Nano **9**, 7027 (2015).
[42] M. Gobbi, F. Golmar, R. Llopis, F. Casanova, and L. E. Hueso, Room-temperature spin transport in C_{60}-based spin valves, Adv. Mater. **23**, 1609 (2011).
[43] Z. H. Xiong, D. Wu, Z. V. Vardeny, and J. Shi, Giant magnetoresistance in organic spin-valves, Nature (London) **427**, 821 (2004).
[44] J. M. Gottfried, Surface chemistry of porphyrins and phthalocyanines, Surf. Sci. Rep. **70**, 259 (2015).
[45] H. Wende, M. Bernien, J. Luo, C. Sorg, N. Ponpandian, J. Kurde, J. Miguel, M. Piantek, X. Xu, P. Eckhold, W. Kuch, K. Baberschke, P. M. Panchmatia, B. Sanyal, P. M. Oppeneer, and O. Eriksson, Substrate-induced magnetic ordering and switching of iron porphyrin molecules, Nat. Mater. **6**, 516 (2007).
[46] E. Annese, G. Di Santo, F. Choueikani, E. Otero, and P. Ohresser, Iron Phthalocyanine and ferromagnetic thin films: Magnetic behavior of single and double interfaces, ACS Omega **4**, 5076 (2019).
[47] H. M. Sturmeit, I. Cojocariu, A. Windischbacher, P. Puschnig, C. Piamonteze, M. Jugovac, A. Sala, C. Africh, G. Comelli, A. Cossaro, A. Verdini, L. Floreano, M. Stredansky, E. Vesselli, C. Hohner, M. Kettner, J. Libuda, C. M. Schneider, G. Zamborlini, M. Cinchetti *et al.*, Room-temperature on-spin-switching and tuning in a porphyrin-based multifunctional interface, Small **17**, 2104779 (2021).
[48] M. Marino, E. Molteni, S. Achilli, and G. Fratesi, *Ab-initio* electronic, magnetic, and optical properties of fe-phthalocyanine on NiO(001), Inorg. Chim. Acta **562**, 121877 (2024).
[49] M. Bernien, J. Miguel, C. Weis, M. E. Ali, J. Kurde, B. Krumme, P. M. Panchmatia, B. Sanyal, M. Piantek, P. Srivastava, K. Baberschke, P. M. Oppeneer, O. Eriksson, W. Kuch, and H. Wende, Tailoring the nature of magnetic coupling of Fe-porphyrin molecules to ferromagnetic substrates, Phys. Rev. Lett. **102**, 047202 (2009).
[50] A. Picone, D. Giannotti, M. Riva, A. Calloni, G. Bussetti, G. Berti, L. Duò, F. Ciccacci, M. Finazzi, and A. Brambilla, Controlling the electronic and structural coupling of C_{60} nano films on Fe(001) through oxygen adsorption at the interface, ACS Appl. Mater. Interfaces **8**, 26418 (2016).

[51] A. Brambilla, A. Picone, D. Giannotti, A. Calloni, G. Berti, G. Bussetti, S. Achilli, G. Fratesi, M. I. Trioni, G. Vinai, P. Torelli, G. Panaccione, L. Duò, M. Finazzi, and F. Ciccacci, Enhanced magnetic hybridization of a spinterface through insertion of a two-dimensional magnetic oxide layer, Nano Lett. **17**, 7440 (2017).

[52] M. S. Jagadeesh, A. Calloni, A. Brambilla, A. Picone, A. Lodesani, L. Duò, F. Ciccacci, M. Finazzi, and G. Bussetti, Room temperature magnetism of ordered porphyrin layers on Fe, Appl. Phys. Lett. **115**, 082404 (2019).

[53] G. Fratesi, S. Achilli, A. Ugolotti, A. Lodesani, A. Picone, A. Brambilla, L. Floreano, A. Calloni, and G. Bussetti, Nontrivial central-atom dependence in the adsorption of M-TPP molecules (M = Co, Ni, Zn) on Fe(001)-$p(1 \times 1)$O, Appl. Surf. Sci. **530**, 147085 (2020).

[54] G. Panaccione, I. Vobornik, J. Fujii, D. Krizmancic, E. Annese, L. Giovanelli, F. Maccherozzi, F. Salvador, A. De Luisa, D. Benedetti *et al.*, Advanced photoelectric effect experiment beamline at elettra: A surface science laboratory coupled with synchrotron radiation, Rev. Sci. Instrum. **80**, 043105 (2009).

[55] P. Giannozzi, O. Andreussi, T. Brumme, O. Bunau, M. B. Nardelli, M. Calandra, R. Car, C. Cavazzoni, D. Ceresoli, M. Cococcioni, N. Colonna, I. Carnimeo, A. D. Corso, S. de Gironcoli, P. Delugas, R. A. DiStasio Jr, A. Ferretti, A. Floris, G. Fratesi, G. Fugallo *et al.*, Advanced capabilities for materials modelling with Quantum ESPRESSO, J. Phys.: Condens. Matter **29**, 465901 (2017).

[56] P. Giannozzi, S. Baroni, N. Bonini, M. Calandra, R. Car, C. Cavazzoni, D. Ceresoli, G. L. Chiarotti, M. Cococcioni, I. Dabo, A. Dal Corso, S. de Gironcoli, S. Fabris, G. Fratesi, R. Gebauer, U. Gerstmann, C. Gougoussis, A. Kokalj, M. Lazzeri, L. Martin-Samos *et al.*, QUANTUM ESPRESSO: A modular and open-source software project for quantum simulations of materials, J. Phys.: Condens. Matter **21**, 395502 (2009).

[57] V. R. Cooper, Van der waals density functional: An appropriate exchange functional, Phys. Rev. B **81**, 161104 (2010).

[58] B. Himmetoglu, A. Floris, S. de Gironcoli, and M. Cococcioni, Hubbard-corrected DFT energy functionals: The LDA+U description of correlated systems, Int. J. Quantum Chem. **114**, 14 (2014).

[59] A. Rohrbach, J. Hafner, and G. Kresse, *Ab initio* study of the (0001) surfaces of hematite and chromia: Influence of strong electronic correlations, Phys. Rev. B **70**, 125426 (2004).

[60] I. E. Brumboiu, S. Haldar, J. Lüder, O. Eriksson, H. C. Herper, B. Brena, and B. Sanyal, Influence of electron correlation on the electronic structure and magnetism of transition-metal phthalocyanines, J. Chem. Theory Comput. **12**, 1772 (2016).

[61] See Supplemental Material at http://link.aps.org/supplemental/10.1103/2pq1-8x4z for further information on the absorption spectra lineshape and for measurements on thick molecular layers, which also includes Refs. [77–83].

[62] K. F. Garrity, J. W. Bennett, K. M. Rabe, and D. Vanderbilt, Pseudopotentials for high-throughput DFT calculations, Comput. Mater. Sci. **81**, 446 (2014).

[63] C. Theil, J. van Elp, and F. Folkmann, Ligand field parameters obtained from and chemical shifts observed at the Cr $L_{2,3}$ edges, Phys. Rev. B **59**, 7931 (1999).

[64] M. Asa, G. Vinai, J. L. Hart, C. Autieri, C. Rinaldi, P. Torelli, G. Panaccione, M. L. Taheri, S. Picozzi, and M. Cantoni, Interdiffusion-driven synthesis of tetragonal chromium (III) oxide on $BaTiO_3$, Phys. Rev. Mater. **2**, 033401 (2018).

[65] S. Fiori, D. Dagur, M. Capra, A. Picone, A. Brambilla, P. Torelli, G. Panaccione, and G. Vinai, Electronically ordered ultrathin Cr_2O_3 on Pt(111) in presence of a multidomain graphene intralayer, Appl. Surf. Sci. **613**, 155918 (2023).

[66] A. Kramer, L. Bignardi, P. Lacovig, S. Lizzit, and M. Batzill, Comparison of surface structures of corundum Cr_2O_3(0001) and V_2O_3(0001) ultrathin films by x-ray photoelectron diffraction, J. Phys.: Condens. Matter **30**, 074002 (2018).

[67] A. Maetaki and K. Kishi, Preparation of ultrathin chromium oxide films on Cu(110) investigated by XPS and LEED, Surf. Sci. **411**, 35 (1998).

[68] M. Marino, E. Molteni, S. Achilli, G. Onida, and G. Fratesi, *Ab initio* electronic, magnetic, and optical properties of Fe phthalocyanine on Cr_2O_3(0001), Molecules **29**, 2889 (2024).

[69] D. J. Coulman, J. Wintterlin, R. J. Behm, and G. Ertl, Novel mechanism for the formation of chemisorption phases: The (2×1)O-Cu(110) "added row" reconstruction, Phys. Rev. Lett. **64**, 1761 (1990).

[70] M. Glaser, H. Peisert, H. Adler, M. Polek, J. Uihlein, P. Nagel, M. Merz, S. Schuppler, and T. Chassè, Transition-metal phthalocyanines on transition-metal oxides: Iron and cobalt phthalocyanine on epitaxial MnO and TiO_x films, J. Phys. Chem. C **119**, 27569 (2015).

[71] D. B. Dougherty, A. Sandin, E. Vescovo, and J. E. Rowe, Coverage-dependent surface magnetism of iron phthalocyanine on an O-Fe(110) surface, Phys. Rev. B **90**, 045406 (2014).

[72] T. Iino, T. Moriyama, H. Iwaki, H. Aono, Y. Shiratsuchi, and T. Ono, Resistive detection of the néel temperature of Cr_2O_3 thin films, Appl. Phys. Lett. **114**, 022402 (2019).

[73] X. Wang, K. Ujimoto, K. Toyoki, R. Nakatani, and Y. Shiratsuchi, Increase of néel temperature of magnetoelectric Cr_2O_3 thin film by epitaxial lattice matching, Appl. Phys. Lett. **121**, 182402 (2022).

[74] H. Sameshima, K. Ujimoto, R. Tsutsumi, K. Toyoki, R. Nakatani, and Y. Shiratsuchi, Finite size effect and dimensional crossover in antiferromagnetic epitaxial Cr_2O_3 thin films, in *2023 IEEE International Magnetic Conference - Short Papers (INTERMAG Short Papers), Sendai, Japan* (IEEE, 2023), pp. 1–2.

[75] F. Motti, G. Vinai, A. Petrov, B. A. Davidson, B. Gobaut, A. Filippetti, G. Rossi, G. Panaccione, and P. Torelli, Strain-induced magnetization control in an oxide multiferroic heterostructure, Phys. Rev. B **97**, 094423 (2018).

[76] S. K. Chaluvadi, S. P. Chalil, A. Jana, D. Dagur, G. Vinai, F. Motti, J. Fujii, M. Mezhoud, U. Lüders, V. Polewczyk, I. Vobornik, G. Rossi, C. Bigi, Y. Hwang, T. Olsen, P. Orgiani, and F. Mazzola, Uncovering the lowest thickness limit for room-temperature ferromagnetism of $Cr_{1.6}Te_2$, Nano Lett. **24**, 7601 (2024).

[77] H. Peisert, I. Biswas, M. Knupfer, and T. Chassé, Orientation and electronic properties of phthalocyanines on polycrystalline substrates, Phys. Status Solidi B **246**, 1529 (2009).

[78] E. Annese, G. Di Santo, F. Choueikani, E. Otero, and P. Ohresser, Formation of a metallic ferromagnetic thin film on top of an FePc-ordered thin film: The chemical and magnetic properties of the interface, J. Phys. Chem. C **123**, 17521 (2019).

[79] J. Uihlein, H. Peisert, H. Adler, M. Glaser, M. Polek, R. Ovsyannikov, and T. Chassé, Interface between FePc and Ni(111): Influence of graphene buffer layers, J. Phys. Chem. C **118**, 10106 (2014).

[80] F. Petraki, H. Peisert, P. Hoffmann, J. Uihlein, M. Knupfer, and T. Chassé, Modification of the 3d-electronic configuration of manganese phthalocyanine at the interface to gold, J. Phys. Chem. C **116**, 5121 (2012).

[81] P. Gargiani, G. Rossi, R. Biagi, V. Corradini, M. Pedio, S. Fortuna, A. Calzolari, S. Fabris, J. C. Cezar, N. B. Brookes, and M. G. Betti, Spin and orbital configuration of metal phthalocyanine chains assembled on the Au(110) surface, Phys. Rev. B **87**, 165407 (2013).

[82] J. Bartolomé, F. Bartolomé, L. M. García, G. Filoti, T. Gredig, C. N. Colesniuc, I. K. Schuller, and J. C. Cezar, Highly unquenched orbital moment in textured Fe-phthalocyanine thin films, Phys. Rev. B **81**, 195405 (2010).

[83] M. Scardamaglia, S. Lisi, S. Lizzit, A. Baraldi, R. Larciprete, C. Mariani, and M. G. Betti, Graphene-induced substrate decoupling and ideal doping of a self-assembled iron-phthalocyanine single layer, J. Phys. Chem. C **117**, 3019 (2013).

[84] A. Brambilla, Dataseta associated to M. Capra *et al.*, Phys. Rev. Mater. 2025, Zenodo (2025), https://doi.org/10.5281/zenodo.17244222.